# Multi-objective dynamic system model for the optimal sizing and real-world simulation of grid-connected hybrid photovoltaic-hydrogen (PV-H2) energy systems.

ATTEYA, A.I., ALI, D. and SELLAMI, N.

2025

energies

MDPI

*Article*

# Multi-Objective Dynamic System Model for the Optimal Sizing and Real-World Simulation of Grid-Connected Hybrid Photovoltaic-Hydrogen (PV-$H_2$) Energy Systems

**Ayatte I. Atteya [1,2], Dallia Ali [1] and Nazmi Sellami [3,*]**

[1] School of Computing, Engineering and Technology, Robert Gordon University, Aberdeen AB10 7GJ, UK; a.atteya@rgu.ac.uk (A.I.A.); d.ali@rgu.ac.uk (D.A.)
[2] Department of Electrical and Control Engineering, College of Engineering and Technology, Arab Academy for Science, Technology and Maritime Transport, Alexandria P.O. Box 1029, Egypt
[3] School of Computing, Engineering and the Built Environment, Edinburgh Napier University, Edinburgh EH10 5DT, UK
* Correspondence: n.sellami@napier.ac.uk

**Abstract:** Hybrid renewable-hydrogen energy systems offer a promising solution for meeting the globe's energy transition and carbon neutrality goals. This paper presents a new multi-objective dynamic system model for the optimal sizing and simulation of hybrid PV-$H_2$ energy systems within grid-connected buildings. The model integrates a Particle Swarm Optimisation (PSO) algorithm that enables minimising both the levelised cost of energy (LCOE) and the building carbon footprint with a dynamic model that considers the real-world behaviour of the system components. Previous studies have often overlooked the electrochemical dynamics of electrolysers and fuel cells under transient conditions from intermittent renewables and varying loads, leading to the oversizing of components. The proposed model improves sizing accuracy, avoiding unnecessary costs and space. The multi-objective model is compared to a single-objective PSO-based model that minimises the LCOE solely to assess its effectiveness. Both models were applied to a case study within Robert Gordon University in Aberdeen, UK. Results showed that minimising only the LCOE leads to a system with a 1000 kW PV, 932 kW electrolyser, 22.7 kg $H_2$ storage tank, and 242 kW fuel cell, with an LCOE of 0.366 £/kWh and 40% grid dependency. The multi-objective model, which minimises both the LCOE and the building carbon footprint, results in a system with a 3187.8 kW PV, 1000 kW electrolyser, 106.1 kg $H_2$ storage tank, and 250 kW fuel cell, reducing grid dependency to 33.33% with an LCOE of 0.5188 £/kWh.

**Keywords:** hybrid renewable-hydrogen energy systems; optimal sizing model; particle swarm optimisation; levelised cost of energy; carbon footprint; cost-optimisation function; cost- and footprint-optimisation function

Academic Editor: Fushou Xie

Received: 27 November 2024
Revised: 3 January 2025
Accepted: 21 January 2025
Published: 25 January 2025

**Citation:** Atteya, A.I.; Ali, D.; Sellami, N. Multi-Objective Dynamic System Model for the Optimal Sizing and Real-World Simulation of Grid-Connected Hybrid PV-$H_2$ Energy Systems. *Energies* **2025**, *18*, 578. https://doi.org/10.3390/en18030578



## 1. Introduction

Hybrid renewable-hydrogen energy systems (HRHESs) are systems which integrate hydrogen energy storage (HES) with renewable sources to allow an energy storage medium for the excess from renewable production in the form of a clean fuel that can be used later when needed during no renewable inputs or deficit production. This stored green hydrogen ($H_2$) can be either used in a fuel cell to supply the load demand with electrical

energy when needed or can be used directly as a fuel for heating purposes or fuelling vehicles [1]. The accurate sizing, energy management, and real-world simulation of such a dynamic hybrid system within grid-integrated buildings represent key challenges for its wider deployment. In this context, researchers have developed single-objective optimisation models [2–6] that allow for the optimal sizing and energy management of standalone or grid-connected HRHESs while aiming for only cost minimisation. However, in their models, they did not consider the dynamic behaviour of the electrolyser in response to the varying renewable energy input or the dynamic behaviour of the fuel cell in response to the dynamic availability of $H_2$ in the storage tank. Further research routes have developed multi-objective optimisation models for grid-integrated HRHESs while aiming for various aspects in their optimisation. Gharibi et al. [7] developed a model that allows for the optimal sizing and power exchange of a grid-connected hybrid system combining a diesel generator, PV arrays, and fuel cell, while aiming for the optimisation of cost, reliability, and renewability. However, their system modelling has notable limitations since the electrolyser was modelled using a fixed molar flow rate for $H_2$ production, which fails to capture dynamic performance changes under variable operating conditions due to fluctuating renewable inputs. Additionally, their fuel cell model does not incorporate electrochemical losses, such as activation, ohmic, or concentration losses, which are critical for accurately predicting the system efficiency and output power. Abdelshafy et al. [8] developed a model that allows for the optimal sizing of a grid-connected desalination power plant powered from hybrid renewables, including PV, wind, a battery, HES, and a diesel backup, while aiming to minimise costs and carbon emissions. However, their system modelling reflects oversimplifications given that the electrolyser and fuel cell models relied on fixed efficiency assumptions, neglecting real-time performance variations due to fluctuating renewable inputs, storage levels, electrochemical losses, and varying load demands. Fonseca et al. [9,10] developed a multi-criteria optimisation model that allows for the optimal design of a distributed energy system incorporating PV panels, a battery, and HES while aiming for optimisation of costs, carbon emissions, and sustainability aspects. However, again, their modelling assumed constant efficiencies for energy conversion units, including the electrolyser and fuel cell, throughout their operation. Furthermore, key aspects such as the faraday efficiency and irreversible losses were completely overlooked, limiting the model's ability to predict the actual $H_2$ production and consumption rates under real-world scenarios, as well as the energy losses and the overall system efficiency. More recently published studies have advanced the integration of hybrid hydrogen batteries within renewable energy microgrids. D. Yousri et al. [11] introduced an integrated energy management system for the optimal scheduling of a hybrid hydrogen battery storage system within a microgrid setup while aiming to minimise the electricity and battery degradation costs, the customers' discomfort, and the peak-to-average ratio. The authors incorporated a detailed electrolyser model into their multi-objective optimisation considering the electrochemical characterisation of the electrolyser cell and the Faraday efficiency. Similarly, B. Modu et al. [12] adopted the same electrolyser cell model for the optimal sizing of a renewable energy microgrid with a hybrid hydrogen and battery storage system while aiming to minimise the annualised system cost and the LCOE. However, both studies relied on a simplistic fuel cell model, treating fuel cell efficiency as a constant parameter and failing to account for voltage losses, real-time dynamics, and load-following behaviour. Further studies have explored the capacity optimisation of hybrid energy storage systems involving HES and batteries within grid-connected integrated energy systems. C. Li et al. [13] proposed a multi-objective optimisation framework for optimising the capacity of a hybrid energy storage system integrating HES with batteries under multiple source-load conditions while aiming to minimise the LCOE and the idle rate of the hybrid energy storage system. While the proposed framework robustly

integrated various scenarios accounting for variability in renewable generation and load demand, the $H_2$ storage system modelling relied on fixed conversion ratios for both the electrolyser and fuel cell. In a similar study [14], Lin et al. developed a two-stage decision-making framework for optimising the capacity of multiple storage schemes comprising HES and batteries while aiming to optimise the LCOE, the power abandonment rate, and the self-sufficiency rate. Although the study introduced life models for HES and batteries and leveraged their complementary characteristics, it exhibited recurring limitations, including the reliance on static efficiency values for the electrolyser and fuel cell, highlighting limited exploration of transient dynamics under real-world scenarios.

In summary, based on the conducted review, a considerable research effort has been done in this area; however, they tended to focus on modelling the energy management among the hybrid system components with less focus on their real-world dynamics. The optimisation of hybrid system sizing highly depends on the mathematical models used for the hybrid system components. The previously presented research often relied on using simplistic hybrid system modelling, which lacked the consideration of the electrochemical dynamic behaviour of electrolysers and fuel cell systems under transient variations imposed by intermittent renewables as well as load changes. This therefore represents a key deviation from finding a real-world optimal sizing solution. Therefore, it is essential to use dynamic mathematical models that represent real-world $H_2$ production by electrolysers and real-world $H_2$ consumption by fuel cells to allow for accurately sizing the storage capacity required, thereby avoiding the oversizing associated with additional costs and space requirements.

This paper addresses this gap in the knowledge by developing a multi-objective dynamic system model for optimally sizing hybrid PV-$H_2$ energy systems. In the developed model, a PSO algorithm is integrated within a novel precise dynamic hybrid system model that takes into consideration the electrochemical losses occurring under the influence of transient load variations and their impact on the output of electrolysers and fuel cell systems. Unlike existing models in the literature research, this dynamic model uniquely captures the variations in the electrolyser's Faraday efficiency each hour based on changes in the PV surplus power fed to the electrolyser and accordingly quantifies the corresponding rate of $H_2$ production. In this way, the dynamic model avoids constant efficiency assumptions or fixed molar flow rates, thus accounting for the impact of real-world performance variations on the quantity of $H_2$ produced. Additionally, modelling of hourly variations in the fuel cell irreversible losses, including activation, ohmic, and concentration losses based on fluctuations in the $H_2$ storage levels, is inclusively integrated into the model. This aspect therefore reflects a variable fuel cell efficiency, thus greatly enhancing the model's ability to predict the actual $H_2$ consumption levels and the fuel cell output power generation. The multi-objective optimisation is performed with respect to two objectives: minimising the LCOE as well as minimising the building carbon footprint. To enable envisioning the impact of using the multiple optimisation criteria on the hybrid system's conceptual design, a single-objective optimal sizing model was firstly developed for minimising the LCOE, and then the multi-objective optimal sizing model was developed for simultaneously minimising both the LCOE and the building carbon footprint. Results from both models are presented and critically analysed with an in-depth discussion. The key innovations and contributions of this paper can be summarised as follows:

- Developing a detailed dynamic hybrid system model that integrates hourly variations in electrolyser Faraday efficiency and fuel cell irreversible losses, avoiding static efficiency assumptions and enabling accurate representation of $H_2$ production and consumption under real-world conditions.
- Integrating a PSO algorithm with the detailed dynamic hybrid system model to optimise the hybrid system sizing from both economic and environmental perspectives.

This integration improves sizing accuracy, avoiding oversizing of the system components associated with unnecessary costs and space.

- Conducting reflective comparative analysis of both the developed single-objective and multi-objective optimal sizing models via implementing them on the same case study building within the Robert Gordon University (RGU) campus in Aberdeen to enable visualising the difference in the system sizing and simulation.

## 2. The Proposed Hybrid PV-$H_2$ Energy System

The proposed hybrid PV-$H_2$ energy system consists of a solar photovoltaic (PV) system, a water electrolyser, a pressurised $H_2$ storage tank, and a fuel cell. The energy management mechanism adopted in the developed system model is designed to ensure that the building's energy needs are primarily met with green energy; therefore, the solar PV system and the fuel cell represent the main power sources serving the building's energy demands. When sunlight is available, the building's demands are mainly supplied by the PV system via an inverter, while any solar energy excess is used to produce green $H_2$ using the electrolyser. It should be noted that the market available electrolysers [15,16] are typically equipped with power supply units featuring built-in rectifiers to convert the AC voltage supply into DC input current. Thus, the electrolyser considered in this study is assumed to have an embedded rectifier to align with the design of commercial electrolysers. The produced $H_2$ is stored as pressurised gas in a tank for later use by the fuel cell. When sunlight is limited or unavailable, the stored $H_2$ is used to power the fuel cell to cover any remaining energy demand. If the PV system and fuel cell cannot fully meet the building's demand with green energy, then the utility grid is allowed to serve the demand that is unmet by the green energy supply (i.e., PV system or fuel cell). Therefore, no battery banks are considered in this configuration to reduce the system costs and complexity, since the hybrid system is grid-connected, and the utility grid provides a backup power when the hybrid system is insufficient to meet the load demand. Any non-utilised excess in PV energy is sold back to the grid to generate additional revenue. Figure 1 illustrates the proposed hybrid PV-$H_2$ energy system with the implemented energy management mechanism.

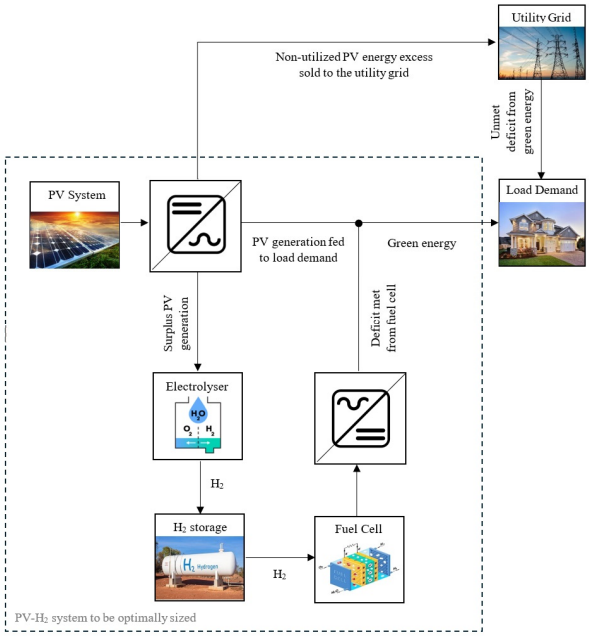


**Figure 1.** Schematic diagram of the proposed hybrid PV-$H_2$ energy system [17].

## 3. Dynamic Modelling of Subsystems

The dynamic modelling of subsystems presented in this paper builds up on methodologies established in our previous research work [18]. Broadly, the dynamic system model has the following main features:

- It is an hourly time-dependent model that considers the hourly variations in PV production and in load consumption over a one-year time interval.
- It is a transient dynamic model that captures the changes in the electrochemical performance characteristics of the electrolyser and fuel cell under real-world operating conditions.
- All components' sizes are treated as continuous variables which are iteratively optimised each algorithmic cycle.
- The inverters' efficiencies are considered to be fixed.

To maintain succinctness in this paper, a concise overview of the key equations representing each subsystem is presented in the following subsections. The full explanation of the mathematical background is provided in our prior publication [18].

### *3.1. Modelling of PV System*

In the PV system model, the hourly net power generated from the PV is determined based on the PV inverter efficiency, the PV size, and the environmental conditions of solar insolation and temperature, as given by Equation (1):

$$P_{PV}^{net}(t) = \eta_{inv}^{PV} . P_{PV} . \frac{G(t)}{G_{STC}} [1 + K_t(T_a(t) + \frac{(NOCT - T_{NOCT}). G_{STC}}{G_{NOCT}} - T_{STC})] \quad (1)$$

where $P_{PV}^{net}(t)$ is the hourly net power generated from the PV system; $\eta_{inv}^{PV}$ is the efficiency of the PV inverter; $P_{PV}$ is the size of the PV system; $G(t)$ is the hourly solar insolation; $G_{STC}$ and $T_{STC}$ are the solar insolation and PV cell temperature at standard test conditions, respectively; $T_a(t)$ is the hourly ambient temperature; $NOCT$ is the nominal operating cell temperature; $G_{NOCT}$ and $T_{NOCT}$ are the solar insolation and ambient temperature which define the $NOCT$, respectively; and $K_t$ is the temperature coefficient of power.

### *3.2. Modelling of Electrolyser*

The electrolyser model simulates the $H_2$ production by converting solar power excess into chemical energy. This incorporates the hourly determination of Faraday efficiency, which reflects the fraction of current being used for producing $H_2$ from the total current supplied to the electrolyser. In the electrolysis of water, a fraction of the overall current is lost in producing unwanted reactions, which is known as 'parasitic currents'. At low current densities, parasitic currents constitute a larger fraction of the overall current because the current supplied is low, meaning less current is being used for splitting the water into $H_2$ and oxygen ($O_2$), and therefore less Faraday efficiency. In contrast, at higher current densities, the fraction of parasitic currents from the overall current diminishes because the current supplied is very high, thus improving Faraday efficiency. Therefore, the magnitude of current supplied to the electrolyser subsystem determines the Faraday efficiency, which changes with the hourly solar power excess. This is modelled using an approximated empirical formula given by Equation (2) depicting how Faraday efficiency dynamically behaves with varying current densities.

$$\eta_F(t) = \frac{(i_{el}(t)/A)^2}{f_1 + (i_{el}(t)/A)^2} f_2 \quad (2)$$

where $\eta_F(t)$ is the hourly Faraday efficiency of the electrolyser, $i_{el}(t)$ is the hourly current supplied to the electrolyser cell (A), $A$ is the area of the electrode ($m^2$), and $f_1$ and $f_2$ are Faraday efficiency parameters.

The relationship between the current supplied to the electrolyser cell, the stack design, and the Faraday efficiency is then used to estimate $H_2$ production rates and thus the hourly amount of $H_2$ generated by the electrolyser, as given by Equation (3). By dynamically adjusting the $H_2$ output in response to hourly changes in Faraday efficiency, the electrolyser model accounts for the impact of hourly parasitic current loss on the amount of $H_2$ produced, reflecting real-world electrolyser behaviour under intermittent renewable energy input.

$$m_{H2g}(t) = \eta_F(t)\frac{n_c\, i_{el}(t)}{2F}.M.N_s^{el}(t).3600 \quad (3)$$

where $m_{H2g}(t)$ is the hourly amount of $H_2$ generated by the electrolyser (kg), $n_c$ is the number of electrolyser cells connected in a series to assemble the electrolyser stack, $N_s^{el}(t)$ is the hourly number of operational electrolyser stacks connected in parallel to assemble the whole electrolyser subsystem, $M$ is the $H_2$ molar mass (kg/mol.), and $F$ is the Faraday constant (C/mol.).

The model also adheres to the electrolyser operational constraints, restricting the power supplied to the electrolyser subsystem from the available solar power excess to only its rated input power in case the former exceeds the latter, where any remainder in solar power excess is sold to the utility grid as ruled by the following equations:

$$P_{el}(t) = \begin{cases} \Delta P(t), & \Delta P(t) \le P_{el} \\ P_{el}, & \Delta P(t) > P_{el} \end{cases} \quad (4)$$

$$P_{ex}^{PV}(t) = \Delta P(t) - P_{el}(t), \;\; \Delta P(t) > P_{el} \quad (5)$$

$$\Delta P(t) = P_{PV}^{net}(t) - P_l(t) \quad (6)$$

where $P_{el}(t)$ is the hourly power supplied to the electrolyser subsystem, $\Delta P(t)$ is the hourly solar power excess, $P_{el}$ is the size of the electrolyser (rated power input to electrolyser), $P_{ex}^{PV}(t)$ is the hourly non-utilised solar power excess sold to the grid, and $P_l(t)$ is the hourly load demand.

### *3.3. Modelling of $H_2$ Storage Tank*

The $H_2$ storage tank model dynamically updates the hourly level of $H_2$ in the storage tank by adding to it the hourly amount of $H_2$ produced by the electrolyser and deducting from it the hourly amount of $H_2$ consumed by the fuel cell, as given by Equation (7).

$$T_{H2}(t) = T_{H2}(t-1) + m_{H2g}(t) - m_{H2c}(t) \quad (7)$$

where $T_{H2}(t)$ is the hourly $H_2$ storage tank level (kg) and $m_{H2c}(t)$ is the hourly amount of $H_2$ consumed by the fuel cell (kg).

### *3.4. Modelling of Fuel Cell*

The fuel cell model simulates two outputs: the fuel cell electrical output power and $H_2$ consumption based on variations in the $H_2$ storage tank levels and in load demand. The molar flow rate of $H_2$ consumption per fuel cell stack is firstly determined based on the currently available $H_2$ storage tank level. This is then used to quantify the hourly fuel cell current using Faraday's law linking the current drawn from the fuel cell stack to the stack design and the molar flow rate of $H_2$ consumption per stack as follows:

$$\dot{n_{H2c}}(t) = n_{fc}.\frac{i_{fc}(t)}{2F} \quad (8)$$

where $\dot{n_{H2c}}(t)$ is the molar flow rate of $H_2$ consumption per fuel cell stack (mol/s), $n_{fc}$ is the number of fuel cells connected in a series to assemble the fuel cell stack, and $i_{fc}(t)$ is the hourly fuel cell current (A).

The electrochemical performance characteristics of the fuel cell are fetched from the stack voltage model, given by Equations (9)–(13), which enables calculating the hourly deviation in the actual cell voltage from its ideal value due to irreversible losses, including activation, ohmic, and concentration losses as a function from the fuel cell current. The model dynamically updates these losses based on operational conditions (i.e., change in hourly fuel cell current), ensuring accurate representation of the fuel cell performance under transient variations.

$$v_{fc}(t) = v_{rev} - v_a(t) - v_o(t) - v_c(t) \tag{9}$$

$$v_{rev} = 1.229 - 0.85 \times 10^{-3}(T - 298.15) + 4.3085 \times 10^{-5}T\ [\ln(P_{H2}) + \frac{1}{2}ln(P_{O2})] \tag{10}$$

$$v_a(t) = -[\xi_1 + \xi_2 T + \xi_3 T\ ln(C_{O2}) + \xi_4 T\ ln\left(i_{fc}(t)\right)] \tag{11}$$

$$v_o(t) = i_{fc}(t)[\ \rho_M(t)\frac{L}{A} + R_c] \tag{12}$$

$$v_c(t) = -\beta\ ln\ (1 - \left(\frac{i_{fc}(t)}{A.j_{max}}\right)) \tag{13}$$

where $v_{fc}(t)$ is the hourly actual fuel cell voltage; $v_{rev}$ is the reversible cell voltage; $v_a(t)$ is the hourly activation loss; $v_o(t)$ is the hourly ohmic loss; $v_c(t)$ is the hourly concentration loss; $T$ is the fuel cell temperature (ºK); $P_{H2}$ and $P_{O2}$ are the partial pressures of $H_2$ and $O_2$ gases (Pa), respectively; $\xi_1, \xi_2, \xi_3, \xi_4$ are parametric coefficients of the fuel cell; $C_{O2}$ is the $O_2$ concentration at the catalytic interface of the cathode (mol/$C^3$); $\rho_M(t)$ is the hourly membrane resistivity (Ω.cm); $A$ is the membrane active area ($cm^2$); $L$ is the membrane thickness (cm); $R_c$ is the resistive coefficient (Ω); $\beta$ is the parametric coefficient (v); and $j_{max}$ is the maximum current density (A/$cm^2$).

The consequent actual fuel cell output power of the whole subsystem is then computed using the actual fuel cell voltage, current, and the subsystem design as given in Equation (14). This value of output power, in turn, is used to calculate the equivalent AC fuel cell output power that can be delivered through the inverter by means of the fuel cell inverter efficiency, as given by Equation (15).

$$P_{fc}^{out}(t) = v_{fc}(t).n_{fc}.i_{fc}(t).N_{fc} \tag{14}$$

$$P_{fc}^{ac}(t) = P_{fc}^{out}(t).\eta_{inv}^{fc} \tag{15}$$

where $P_{fc}^{out}(t)$ is the hourly output voltage across the fuel cell subsystem, $N_{fc}$ is the maximum number of fuel cell stacks connected in parallel to assemble the whole fuel cell subsystem, $P_{fc}^{ac}(t)$ is the hourly equivalent AC fuel cell output power that can be delivered through the inverter, and $\eta_{inv}^{fc}$ is the efficiency of the fuel cell inverter.

To account for the load-following behaviour, the hourly equivalent AC fuel cell output power delivered through the inverter is adjusted to only meet the unmet load demand from the PV system while not exceeding the capacity it could deliver, as given by Equation (16). In case the unmet load demand surpasses the AC equivalent fuel cell output power, the remainder will be supplied from the utility grid, as given by Equation (17).

$$P_{fc}^{ac}(t) = \begin{cases} P_{un}(t), & P_{un}(t) \le P_{fc}^{ac}(t) \\ P_{fc}^{ac}(t), & P_{un}(t) > P_{fc}^{ac}(t) \end{cases} \tag{16}$$

$$P_{grid}(t) = P_{un}(t) - P_{fc}^{ac}(t), \quad P_{un}(t) > P_{fc}^{ac}(t) \tag{17}$$

$$P_{un}(t) = P_l(t) - P_{PV}^{net}(t) \tag{18}$$

where $P_{un}(t)$ is the hourly unmet load demand from the PV system and $P_{grid}(t)$ is the hourly power imported from the utility grid.

Finally, the hourly number of active fuel cell stacks connected in parallel to assemble the fuel cell subsystem for delivering this AC equivalent output power is computed using Equation (19), which is then used to calculate the hourly amount of $H_2$ to be consumed by the fuel cell using Equation (20).

$$N_{fc}(t) = \frac{P_{fc}^{ac}(t)}{\eta_{inv}^{fc}.\, v_{fc}(t).\, n_{fc}.\, i_{fc}(t)} \tag{19}$$

$$m_{H2c}(t) = \dot{n_{H2c}}(t).\, M.\, N_{fc}(t).\, 3600 \tag{20}$$

where $N_{fc}(t)$ is the hourly number of operational fuel cell stacks connected in parallel to assemble the fuel cell subsystem for delivering the corresponding AC equivalent output power.

## 4. Formulating the Objective Functions and Constraints for the Optimal Sizing of Hybrid PV-$H_2$ Energy Systems

In the optimal sizing of hybrid renewable energy systems, the formulation of objective function depends on the design goals, which could be technical, economic, or environmental goals. In terms of technical goals, the reliability of the energy system is the main concern. A hybrid energy system is reliable when it is capable of providing enough power supply to a load demand over a certain period [19]. Referring to the proposed hybrid PV-$H_2$ energy system, the system reliability is considered through the energy balancing mechanism, which is set to enforce feeding the load demand by the green energy supply, and only the load demand that is unmet by the green energy supply is fed from the utility grid. With the technical aspect already considered, the objective function for optimising the proposed hybrid PV-$H_2$ energy system sizing is therefore formulated to consider the economic and environmental aspects. The nature of the objective function depends on the scope of the investors (i.e., whether their focus is financial benefits and/or environmental outcomes). To allow for meeting different decision-making aims, both single-objective and multi-objective optimisation functions are considered in this paper to allow for separate and simultaneous minimisation of the system costs and carbon footprint.

### *4.1. Formulating Single-Objective Cost-Optimisation Function for Optimally Sizing Hybrid PV-$H_2$ Energy Systems from an Economic Perspective*

When optimally sizing the proposed hybrid PV-$H_2$ energy system from an economic perspective, the main objective is to minimise the LCOE of the total energy consumed, which is given by Equation (21). The decision variables are the sizes of the system components, which include the PV system size, electrolyser size, $H_2$ storage tank size, and fuel cell size. The objective is to determine the optimal hybrid system sizing that can minimise the LCOE of the total energy consumed.

$$LCOE = \frac{CRF.\sum_{j=1}^{N_c} NPC_j + C_{grid} - R_{PVsale}}{\sum_{t=1}^{8760} P_l\,(t)} \tag{21}$$

$$CRF = \frac{i(1+i)^N}{(1+i)^N - 1} \tag{22}$$

where $LCOE$ is the levelised cost of energy (£/kWh), $NPC_j$ is the net present costs of component (j) in (£), $j$ represents each individual component in the hybrid system, $N_c$ is the total number of hybrid system components, $C_{grid}$ is the cost of grid import (£), $R_{PVsale}$ is the revenue from selling non-utilised solar energy excess to the grid (£), $P_l(t)$ is the hourly building load demand, $CRF$ is the capital recovery factor [4,5,7], $i$ is the real interest rate, and $N$ is the project lifetime.

To enable calculating the LCOE as given by Equation (21), a detailed 'Cost Model' was developed for calculating the net present cost of the hybrid system components. The NPC of each individual hybrid system component is given by Equations (23)–(28) [8] and considers several factors; this includes the component's capital cost, the component's operation and maintenance costs over the project's lifetime, the component's replacement cost if the component's lifespan is shorter than the project's lifetime, and the component's salvage value. The latter denotes the revenue generated from the component's remaining lifespan at the end of the project lifetime. Therefore, the NPC of each individual hybrid system component is the sum of the component's capital cost, operation and maintenance costs, and replacement cost minus the component's salvage value.

$$NPC_j = C_j^{cap}.P_j + C_j^{OM}.P_j.\sum_{k=1}^{N}\frac{1}{(1+i)^k} + C_{t\,j}^{rep} - C_j^{salv} \tag{23}$$

$$C_{t\,j}^{rep} = \begin{cases} 0, & L_j \geq N \\ C_{PV}^{rep}.P_j.\sum_{n=1}^{r_j}\frac{1}{(1+i)^{L_j*n}}, & L_j < N \end{cases} \tag{24}$$

$$r_j = int\left(\frac{N}{L_j}\right) \tag{25}$$

$$C_j^{salv} = C_{t\,j}^{rep}.\frac{R_j}{j} \tag{26}$$

$$R_j = L_j - (N - D_j) \tag{27}$$

$$D_j = L_j.r_j \tag{28}$$

where $C_j^{cap}$ and $C_j^{OM}$ are the capital cost and the operation and maintenance cost of component (j) per unit rating (£/kW), respectively; $P_j$ is the size of component (j) (kW); $C_{t\,j}^{rep}$ is the total replacement cost of component (j) (£); $C_j^{salv}$ is the salvage value of component (j) (£); $C_j^{rep}$ is the replacement cost of component (j) per unit rating (£/kW); $L_j$ is the lifespan of component (j) (yr.); $r_j$ is the number of replacements of component (j) over the project lifetime rounded down to nearest integer; $R_j$ is the remaining lifespan of component (j) at the end of the project lifetime (yr.); and $D_j$ is the duration of replacement of component (j) (yr.).

The cost of importing electricity from the utility grid and the revenue generated from selling non-utilised solar energy excess to the utility grid are determined using Equations (29) and (30).

$$C_{grid} = \sum_{t=1}^{8760} t_{gp}\,(t).P_{grid}(t) \tag{29}$$

$$R_{PVsale} = t_{gf}.\sum\nolimits_{t=1}^{8760} P_{ex}^{PV}(t) \tag{30}$$

where $t_{gp}$(t) is the hourly tariff rate of electricity purchased from the utility grid considering variable day/night tariff rates, $t_{gf}$ is the tariff rate of grid feed-in electricity, $P_{grid}(t)$ is the power imported from the utility grid at time step (t), and $P_{ex}^{PV}(t)$ is the non-utilised solar power excess at time step (t).

### *4.2. Formulating a Multi-Objective Cost and Footprint Optimisation Function for Optimally Sizing Hybrid PV-H₂ Energy Systems from Both Economic and Environmental Perspectives*

A key controversial issue in designing hybrid renewable energy systems is achieving the lowest $CO_2$ emissions at the lowest cost. For optimally sizing the proposed hybrid PV-$H_2$ energy system from both economic and environmental perspectives, the first objective is to minimise the LCOE of the total energy consumed, as emphasised in Section 3.1, while the second objective is to minimise the carbon footprint of the building considered. This can be measured in terms of the amount of $CO_2$ emissions eliminated upon integrating the proposed hybrid system within the building considered. The more $CO_2$ emissions are eliminated, the more environmentally friendly the building is. Instead of maximising the eliminated $CO_2$ emissions, the $CO_2$ emissions can be minimised through reducing the grid energy import requirements (i.e., minimise dependency on the utility grid). Therefore, the grid dependency ratio (GDR), which is defined as the fraction of load demand that is served from the utility grid over the total load demand, is set as the second objective function to be minimised. Equation (31) is used to calculate the system's GDR, which is proportional to the $CO_2$ emissions associated with the grid energy import requirements; therefore, minimising this factor will consequently minimise the building's carbon footprint.

$$GDR = \frac{\sum_{t=1}^{8760} P_{grid}(t)}{\sum_{t=0}^{8760} P_l(t)} \quad (31)$$

where $GDR$ is the grid dependency ratio and $P_l(t)$ is the building load demand at time step (t).

The multi-objective cost and footprint optimisation function proposed for optimising the sizing of the hybrid PV-$H_2$ energy system from both economic and environmental perspectives simultaneously minimise the LCOE of the total energy consumed as the economic metric and the building's GDR as the environmental metric. The overall objective function is constructed considering the weighted sum method, which allows for assigning each objective a weighting factor based on its relative importance (i.e., priority) for the decision maker [20].

The decision variables remain the sizes of the PV system, electrolyser, $H_2$ storage tank, and fuel cell; however, the objective is to determine the optimal hybrid system sizing that can simultaneously minimise the LCOE along with the building's GDR.

Both the single-objective and multi-objective functions are subject to the inequality constraint given by Equation (32). This constraint represents the boundary limitations of each decision variable (i.e., each individual component in the hybrid system) from which the range of feasible solutions is encountered [4,5,7,8].

$$P_{j\,min} \le P_j \le P_{j\,max} \quad (32)$$

where $P_{j\,min}$, $P_{j\,max}$ are, respectively, the minimum and maximum boundary sizes of component (j). This constraint applies for each of the four decision variables (i.e., the PV system size, electrolyser size, $H_2$ storage tank size, and fuel cell size).

## 5. Development of Both the Single-Objective and Multi-Objective Optimal Sizing Models

In this research work, the PSO algorithm is used with both the single-objective and multi-objective optimisation functions detailed earlier in Section 4. To allow the optimal sizing of the hybrid PV-$H_2$ energy system while considering the real-world dynamics of its individual components, the PSO algorithm is integrated with the dynamic system modelling emphasised in Section 3 and elaborated in earlier research work [18]. The following subsection provides a brief overview of the PSO algorithm implemented in this study.

### *5.1. The PSO Algorithm*

The PSO algorithm is inspired by the animal behaviour of creatures such as birds or fish searching for food or corn by adjusting their positions and velocities within a search space [21]. These animals move as a 'swarm', which stands for the irregular movement of individuals in a search space. Each partner in the swarm is called a 'particle' [8]. The particles in the swarm update their positions and velocities using Equations (33) and (34) [22], based on both their personal experiences and their neighbourhood experiences, towards the global optimal solution.

$$V_i^{k+1} = w \cdot V_i^k + c_1 \cdot rand_1 \cdot P_{best\,i}^k + c_2 \cdot rand_2 \cdot \left(G_{best}^k - X_i^k\right) \quad (33)$$

$$X_i^{k+1} = X_i^k + V_i^{k+1} \quad (34)$$

$$w = \frac{(w_{max} - w_{min})}{k_{max}} * k \quad (35)$$

where $i$ is the number of particles in the swarm; $k$ is the iteration number; $V_i^k$ is the velocity of particle ($i$) at iteration ($k$); $P_{best\,i}^k$ is the best position for particle ($i$) based on its personal experience at iteration ($k$), referred as personal best; $G_{best}^k$ is the best position achieved by the entire particles in the swarm at iteration ($k$), referred as global best; $X_i^k$ is the position of particle ($i$) at iteration ($k$); $c_1, c_2$ are acceleration constants controlling the movement of particles towards $P_{best\,i}^k$ and $G_{best}^k$; $rand_1$, $rand_2$ are random numbers ranging from (0–1); $w$ is the inertia weight factor; $w_{min}$, $w_{max}$ are the minimum and maximum inertia weights; and $k_{max}$ is the maximum number of iterations.

For optimally sizing the hybrid PV-$H_2$ energy system either from an economic perspective, or from both economic and environmental perspectives, each particle's position is represented by a specific configuration of the hybrid system's sizing consisting of the following four decision variables: the PV system size, the electrolyser size, the $H_2$ storage tank size, and the fuel cell size.

### *5.2. Rationale of Selecting the PSO Algorithm*

While the PSO algorithm is traditionally recognised for its effectiveness in solving single-objective optimisation problems, this study further extends its application, in conjunction with the weighted sum method, for multi-objective optimisation tasks. The weighted sum method aggregates multiple objectives into one scalar composite function by assigning each objective a weighting factor based on its relative importance for the decision maker. Compared to traditional pareto-dominance-based algorithms (i.e., Non-dominated Sorting Genetic Algorithm (NSGA-II), Non-dominated Sorting Whale Optimisation Algorithm (NSWOA), etc.), this approach allows for reducing the computational burden, providing faster convergence while still achieving a balance between conflicting objectives. Moreover, it leverages the PSO strengths in exploring high-dimensional search spaces while maintaining simplicity and adaptability to both single-objective and multi-objective optimisation tasks. However, a key limitation of the weighted sum method is

that it relies on pre-determined weighting factors, which require multiple runs to capture a broader range of trade-offs. In contrast, pareto-dominance-based algorithms inherently explore diverse trade-offs; however, they are computationally intensive and less straightforward to implement, particularly for dynamic systems with high-dimensional search spaces. Table 1 summarises the comparison between the implemented PSO in conjunction with the weighted sum method and the traditional pareto-dominance-based algorithms.

**Table 1.** Comparison of the implemented PSO algorithm versus traditional pareto-dominance based algorithms.

| Criteria | The implemented PSO in conjunction with the weighted sum method | Pareto-dominance-based algorithms (i.e., NSGA II, NSWOA, etc.) |
|---|---|---|
| Handling objectives | Aggregates multiple objectives into a single composite function using pre-defined weighting factors | Treats each objective separately and evaluates solutions based on pareto dominance |
| Pareto-front solution | - Provides a single optimal solution per single run<br>- Requires multiple runs to produce a pareto-front set of solutions | Produces a pareto front of diverse trade-off solutions in a single run |
| Ease of implementation | Simple and straightforward to implement | More complex due to multi-objective sorting and diversity maintenance mechanisms |
| Computational burden | Less computational burden | High computational burden |
| Convergence speed | Faster convergence | Slower convergence |
| Diversity | Limited diversity | High diversity |

### *5.3. Integrating the PSO Algorithm with the Dynamic Hybrid PV-$H_2$ Energy System Model for Optimising the Hybrid System Sizing from Both Economic and Environmental Perspectives*

Both the single-objective and multi-objective optimal sizing models are developed by implementing the PSO algorithm on the dynamic model of real-world hybrid PV-$H_2$ energy systems provided in Section 3. The following steps were performed to minimise the single-objective or the multi-objective optimisation functions:

**Step 1: Filtration of the Initial Particles' Positions.**

Before beginning to minimise the relevant objective function, the initial search space is subject to a filtration process so that at least 40% of the building's load demand is met by clean energy (i.e., PV system or fuel cell). This baseline is chosen to prioritise sustainability and decarbonisation goals, allowing for a balance between environmental and economic feasibility. From an environmental perspective, the 40% threshold ensures that a significant contribution from clean energy sources is satisfied, reducing the reliance on the electricity grid and, therefore, lowering carbon emissions. From an economic perspective, the 40% threshold avoids too challenging or restrictive constraints that would require significantly larger PV or $H_2$ storage capacities, making the system impractical or excessively expensive. Thus, starting with a moderate threshold allows for the optimisation algorithm to explore configurations which strike a balance between affordability and sustainability. While the global optimal solution might not necessarily depend on the initial generation, this filtration process shifts the focus of the searching space towards configurations favouring cleaner energy. By filtering the initial generation in this manner, the updated particles are guided towards solutions that align with sustainability goals, setting the scene for the optimisation process to further increase the clean energy supply. An initial configuration of the hybrid system sizing is generated from the range of feasible solutions then this initial configuration is tested by applying to it the precise dynamic hybrid system

model described in Section 3 to determine the portion of the load demand supplied by clean energy. If this portion is 40% or more, the configuration is accepted as the initial generation. If not, the system sizing is repeatedly re-generated until at least 40% of the load demand is covered by clean energy.

**Step 2: Identification of Personal Best and Global Best of Filtered Initial Positions.**

The relevant objective function is then computed for each filtered particle's position and evaluated to determine the particle's personal best $(P_{best\,i}^{k})$ and the global best position $(G_{best}^{k})$, which are then used to update the filtered initial particles' positions and velocities using (33) and (34), respectively.

**Step 3: Application of Position Control on Updated Particles' Positions.**

To ensure that the updated values of the hybrid system sizing configuration (i.e., each decision variable in $X_i^k$) remain within their predefined minimum and maximum limits, a position control mechanism is applied as follows: if the updated decision variable lies between these boundaries, then the updated value of this variable is retained, while if the updated decision variable exceeds its boundaries, it reverts to its value from the previous iteration.

**Step 4: Identification of Personal Best and Global Best of Updated Particles' Positions.**

The relevant objective function is computed for each updated particle's position through re-applying to it the precise dynamic hybrid system model detailed in Section 3. The computed objective function for each updated particle's position is then evaluated to update the particle's personal best $(P_{best\,i}^{k})$ and global best position $(G_{best}^{k})$.

**Step 5: Update Particles' Positions and Velocities.**

Equations (33) and (34) are used to update the particles' positions and velocities using the updated values of $P_{best\,i}^{k}$ and $G_{best}^{k}$.

**Step 6: Check the Algorithm Closing Condition.**

If the iteration loop is exhausted, then it terminates. Otherwise, steps 3 to 6 are repeated. It should be noted that the maximum number of iterations must be large enough to allow for the global optimal solutions to stabilise over a series of consecutive iterations, indicating that the solution converges to the global optimal or near-optimal solution. This can be demonstrated through the convergence of a fitness function plot which will be discussed later in Section 6.2.

## 6. Applying the Developed Single-Objective and Multi-Objective Optimal Sizing Models: Case Study of Robert Gordon University Campus Building in Scotland

Both the single- and multi-objective optimal sizing models were applied to a grid-connected case study building within the RGU campus in Aberdeen, Scotland, to enable supporting the university's carbon reduction initiative with the aim of significantly reducing its emissions from energy and consumables. The case study grid-connected building selected was the Riverside Building (RB), which covers three schools and a learning centre. With the help of RGU Estates, the data for the building's energy consumption were carefully collected on an hourly basis throughout a one-year timescale and used in the developed models to enable optimising the sizing of the hybrid PV-$H_2$ energy system components to meet the single- or the multiple-objective optimisation criteria depending on the choice of the decision maker.

### *6.1. Data Collection*

The hourly data collected for the building's energy consumption is as shown in Figure 2a. The building's yearly energy consumption is 1487 MWh, the building's average

hourly power consumption is 170 kW, and the building's peak hourly power consumption is 274 kW. The hourly data of atmospheric conditions at the building location (Aberdeen city) are as shown in Figure 2b. These include the hourly data for solar insolation and ambient temperature at the building location, which were collected from PVGIS web interface.

Table 2 includes all the data required to run both the developed single-objective and multi-objective optimal sizing models. These include the cost parameters required to compute the net present cost of each hybrid system component, with per-unit cost parameters derived from market data in [7], the lifetimes of the hybrid system components [4,7,23], the project lifetime, and the real interest rate considered in this study. Table 3 shows the tariff rates for purchasing electricity from the utility grid and the grid feed-in tariff rates. It should be noted that the data collected for the grid tariff rates and grid feed-in tariff rates were based on the electricity prices of the RGU's UK energy provider for North Scotland considering day and night tariffs [24], while the grid feed-in tariff corresponds to the Smart Export Guarantee (SEG) export rate from the same energy provider [25]. The parameters used for the precise dynamic modelling of the electrolyser, $H_2$ storage tank, and fuel cell can be found in [18].

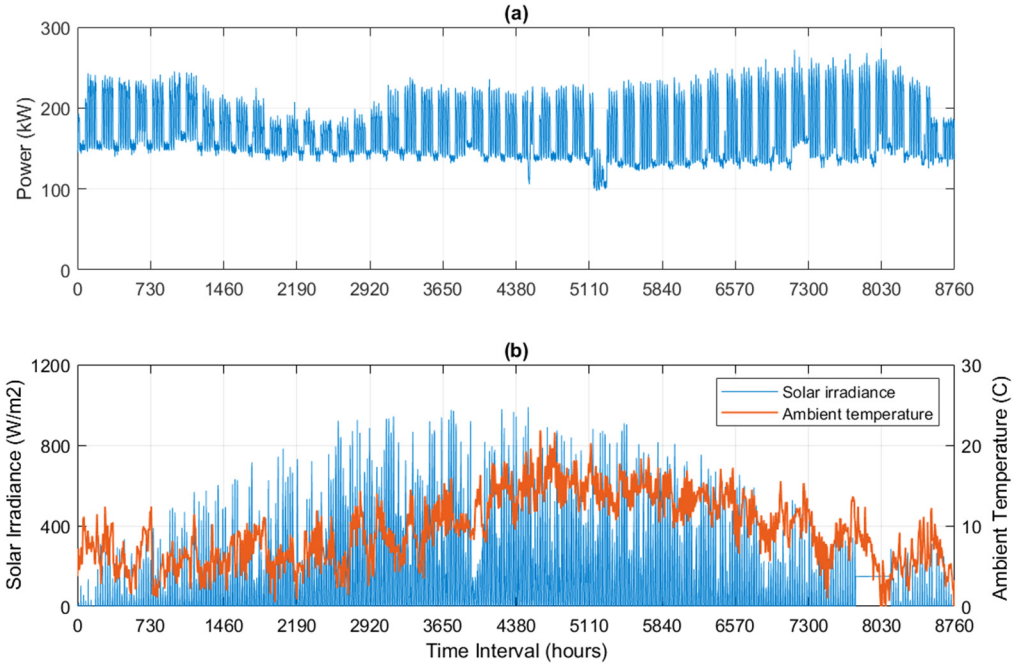


**Figure 2.** (**a**) The hourly data collected for the RB's energy consumption over a one-year timescale and (**b**) the hourly data collected for the solar insolation and the ambient temperature at the building location (Aberdeen City) over a one-year timescale. * The load data presented in this study correspond to the RB at the RGU campus, which has distinct characteristics compared to other buildings analysed in previous studies at the same campus.

**Table 2.** Data required for running both the single-objective and multi-objective optimal sizing models [17].

| Parameter | Description | Value |
|---|---|---|
| $C_{PV}^{cap}$ | Capital cost of PV system per unit rating | 1440 £/kW |
| $C_{PV}^{OM}$ | Operation and maintenance cost of PV system per unit rating | 28.8 £/kW |
| $C_{PV}^{rep}$ | Replacement cost of PV system per unit rating | 1440 £/kW |
| $L_{PV}$ | Lifetime of PV system | 20 years |
| $C_{ele}^{cap}$ | Capital cost of electrolyser per unit rating | 1600 £/kW |

| | | |
|---|---|---|
| $C_{ele}^{OM}$ | Operation and maintenance cost of electrolyser per unit rating | 32 £/kW |
| $C_{ele}^{rep}$ | Replacement cost of electrolyser per unit rating | 1200 £/kW |
| $L_{ele}$ | Lifetime of electrolyser | 15 years |
| $C_{HT}^{cap}$ | Capital cost of $H_2$ storage tank per unit rating | 528 £/kg |
| $C_{HT}^{OM}$ | Operation and maintenance cost of $H_2$ tank per unit rating | 10.56 £/kg |
| $C_{HT}^{rep}$ | Replacement cost of $H_2$ storage tank per unit rating | 528 £/kg |
| $L_{HT}$ | Lifetime of $H_2$ storage tank | 20 years |
| $C_{FC}^{cap}$ | Capital cost of fuel cell per unit rating | 2400 £/kW |
| $C_{FC}^{OM}$ | Operation and maintenance cost of fuel cell per unit rating | 48 £/kW |
| $C_{FC}^{rep}$ | Replacement cost of fuel cell per unit rating | 2000 £/kW |
| $L_{FC}$ | Lifetime of fuel cell | 50,000 h |
| $C_{inv1}^{cap}, C_{inv2}^{cap}$ | Capital cost of PV inverter and fuel cell inverter per unit rating, respectively | 80 £/kW |
| $C_{inv1}^{OM}, C_{inv2}^{OM}$ | Operation and maintenance cost of PV inverter and fuel cell inverter per unit rating, respectively | 1.60 £/kW |
| $C_{inv1}^{rep}, C_{inv2}^{rep}$ | Replacement cost of PV inverter and fuel cell inverter per unit rating, respectively | 80 £/kW |
| $L_{inv1,}L_{inv2}$ | Lifetime of PV inverter and fuel cell inverter, respectively | 15 years |
| $N$ | Project lifetime | 20 years |
| $i$ | Real interest rate | 8% |

**Table 3.** Tariff rates of grid electricity purchase and grid feed-in electricity based on prices of RGU's UK energy provider [17].

| Parameter | Description | Value |
|---|---|---|
| $t_{gp}$ | Tariff rate for grid electricity purchase | Day rate (7.00—12.00 am): 0.4598 £/kWh |
| | | Night rate (12.00–7.00 am): 0.1420 £/kWh |
| $t_{gf}$ | Tariff rate of grid feed-in electricity | 0.056 £/kWh |

*6.2. Results and Discussions*

The PSO algorithm was applied to the RB using a population size of 20 particles and a maximum number of iterations of 50. Table 4 shows the optimal sizing results of the hybrid PV-$H_2$ energy system suited for the RB using both the single-objective optimal sizing model for minimising the LCOE and the multi-objective optimal sizing model for simultaneously minimising the LCOE along with the building's carbon footprint. From Table 4, it can be seen that when using the single-objective optimal sizing model for minimising the LCOE, the optimal hybrid system sizing was found to be a 1000 kW PV system, 932 kW electrolyser, 22.7 kg pressurised $H_2$ storage tank, and 242 kW fuel cell. The LCOE corresponding to this optimal hybrid system sizing was found to be 0.366 £/kWh, while the corresponding building's GDR was found to be 40%. On the other hand, when using the multi-objective optimal sizing model for simultaneously minimising both the LCOE and the building's carbon footprint, the optimal hybrid system sizing was found to be a 3187.8 kW PV system, 1000 kW electrolyser, 106.1 kg $H_2$ storage tank, and 250 kW fuel cell system. The LCOE corresponding to this optimal hybrid system sizing was found to be 0.5188 £/kWh, while the building's GDR was reduced to 33.33%. Compared to the results obtained from the single-objective optimal sizing model, it can be seen that the LCOE was quite higher when using the multi-objective optimal sizing model to enable minimising the GDR in addition to minimising the LCOE. The higher LCOE is because of the higher capacities of hybrid system components needed to allow for increasing the clean energy supply to achieve a lower grid dependency of 33.33% (i.e., 66.67% of the total annual load demand has to be fed by the clean energy supply).

Figure 3 shows the convergence of the fitness function obtained from the single-objective optimal sizing model for minimising the LCOE. As can be seen from Figure 3, the LCOE dropped from about 0.405 £/kWh at the filtered initial hybrid system sizing to 0.366 £/kWh at the optimal hybrid system sizing, thus achieving about a 9.6% reduction in the LCOE after almost 20 iterations (i.e., meaning the solution converges after about 20 iterations). Figure 4 illustrates the pareto-front characteristic of the multi-objective optimal sizing model, showing a trade-off between the LCOE and the building's GDR. It is obvious from the chart that decreasing the building's GDR is associated with an increase in the LCOE and vice versa.

**Table 4.** Results of both the developed single-objective and multi-objective optimal sizing models for RB.

| Parameter | Single-Objective Optimal Sizing Model's Results | Multi-Objective Optimal Sizing Model's Results |
|---|---|---|
| PV system size (kW) | 1000 | 3187.8 |
| Electrolyser size (kW) | 932 | 1000 |
| $H_2$ storage tank size (kg) | 22.7 | 106.1 |
| Fuel cell system size (kW) | 242 | 250 |
| LCOE (£/kWh) | 0.366 | 0.5188 |
| GDR (%) | 40% | 33.33% |

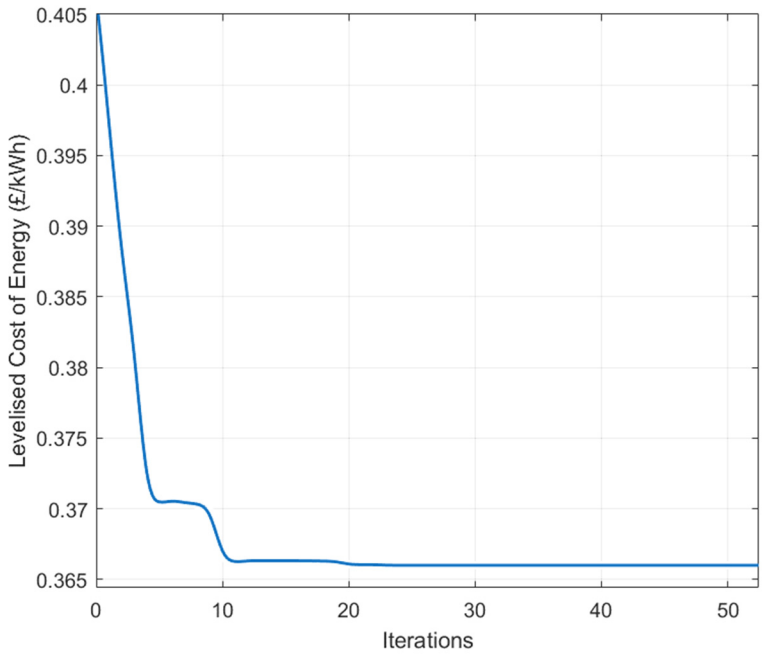


**Figure 3.** Convergence of fitness function of the single-objective optimal sizing model.

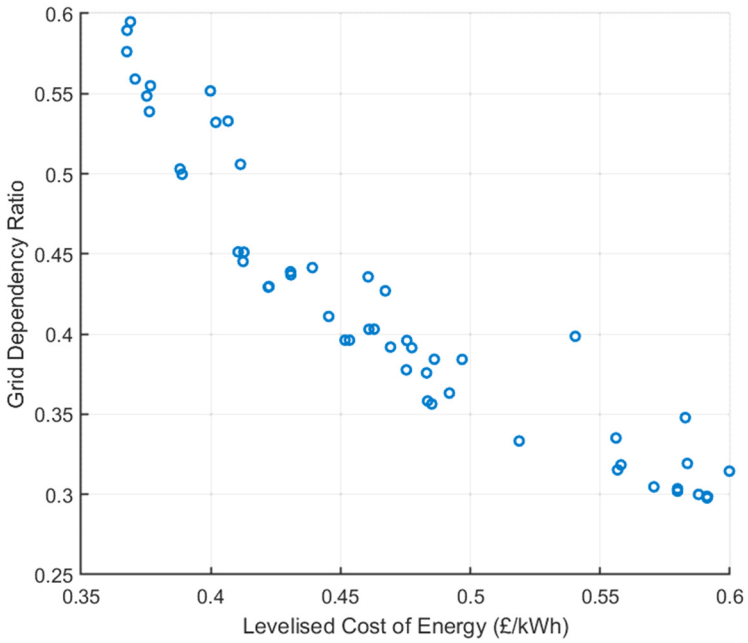


**Figure 4.** Pareto-front characteristic of the multi-objective optimal sizing model.

Figure 5 shows the monthly PV energy production obtained from the optimal hybrid system sizing when using the single-objective optimal sizing model. From Figure 5, the total annual PV energy production was found to be 876.28 MWh when using the single-objective optimal sizing model, out of which 536.4 MWh were fed to the building load demand, while the remainder (i.e., 339.8 MWh) was harnessed by the electrolyser. It is further noted that no PV energy excess was sold to the utility grid when using the single-objective optimal sizing model, meaning the annual PV energy production was fully utilised for feeding the building load demand and the electrolyser to generate green $H_2$.

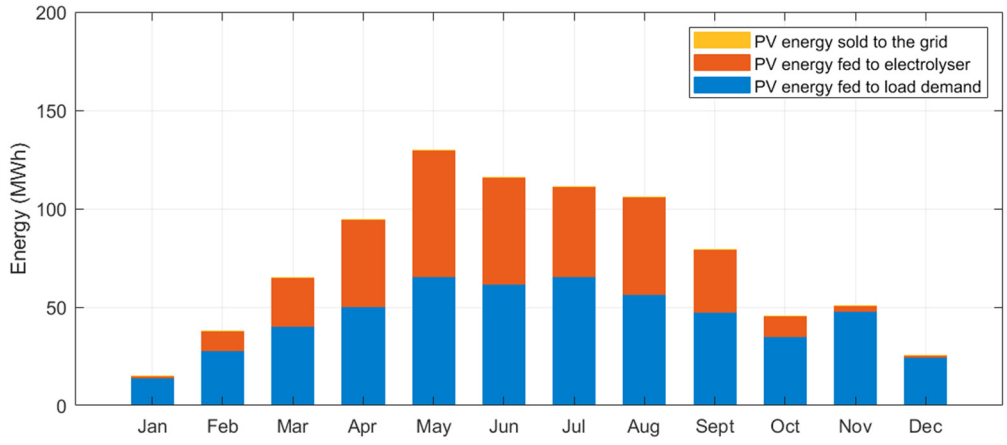


**Figure 5.** Monthly PV energy production obtained from the optimal hybrid system sizing when using the single-objective optimal sizing model.

Figure 6 shows the monthly PV energy production obtained from the optimal hybrid system sizing when using the multi-objective optimal sizing model. From Figure 6, the total annual PV energy production was found to be 2793.45 MWh when using the multi-objective optimal sizing model, out of which 709.81 MWh was fed to the building load demand, 1726.5 MWh was harnessed by the electrolyser, and the remainder of non-utilised PV energy excess was sold to the utility grid (i.e., about 357.13 MWh). Compared to

the results of the single-objective optimal sizing model, the annual PV energy production greatly increased when using the multi-objective optimal sizing model given that a higher capacity of the PV system was obtained, as listed in Table 4. It can be seen that in the multi-objective optimisation, the PSO algorithm increased the capacity of the PV system to enable a greater clean energy supply and to allow for harnessing more PV surplus by the electrolyser and thus increasing the $H_2$ availability for fuel cell consumption. When using the multi-objective optimal sizing model, it can be seen that about 61.8% from annual PV production was harnessed by the electrolyser (i.e., 1726.5 MWh out of 2793.45 MWh), while when using the single-objective optimisation algorithm, only 38.7% from annual PV production was harnessed by the electrolyser (i.e., 339.8 MWh out of 876.28 MWh). In terms of the PV energy excess sold to the utility grid, it can be seen that the multi-objective optimisation allowed for about 12.7% of the annual PV energy production to be sold to the utility grid as a result of the higher PV system capacity, thus increasing the revenue from selling the non-utilised PV energy excess and allowing for maintaining the system's LCOE at a reasonable value.

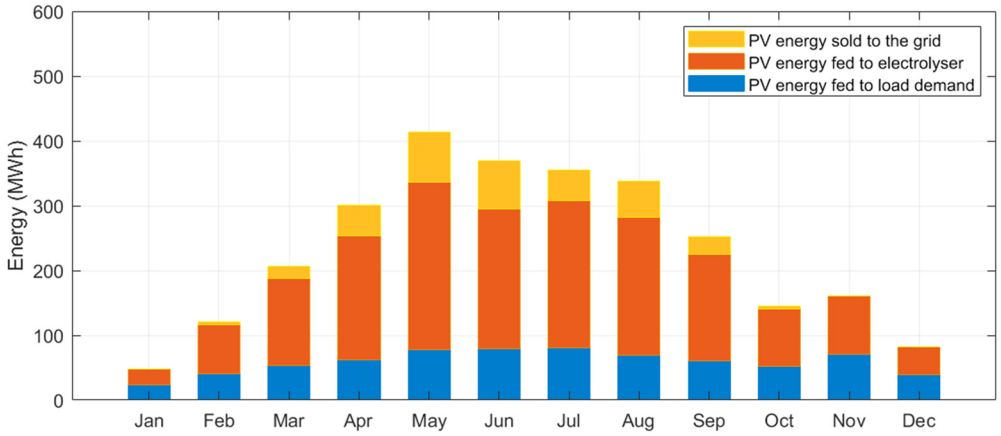


**Figure 6.** Monthly PV energy production obtained from the optimal hybrid system sizing when using the multi-objective optimal sizing model.

Figure 7 compares the monthly $H_2$ production by the electrolyser obtained from the optimal hybrid system sizing when using the single-objective optimal sizing model versus that obtained when using the multi-objective optimal sizing model. Compared to the single-objective optimisation, the total annual $H_2$ production by the electrolyser was noticeably increased when using the multi-objective optimisation algorithm given that more PV surplus power became available for green $H_2$ generation (10,290 kg of $H_2$ was produced by the electrolyser annually from the PV surplus production when using the multi-objective optimisation algorithm, while only 1823.5 kg of $H_2$ was produced when using the single-objective optimisation algorithm).

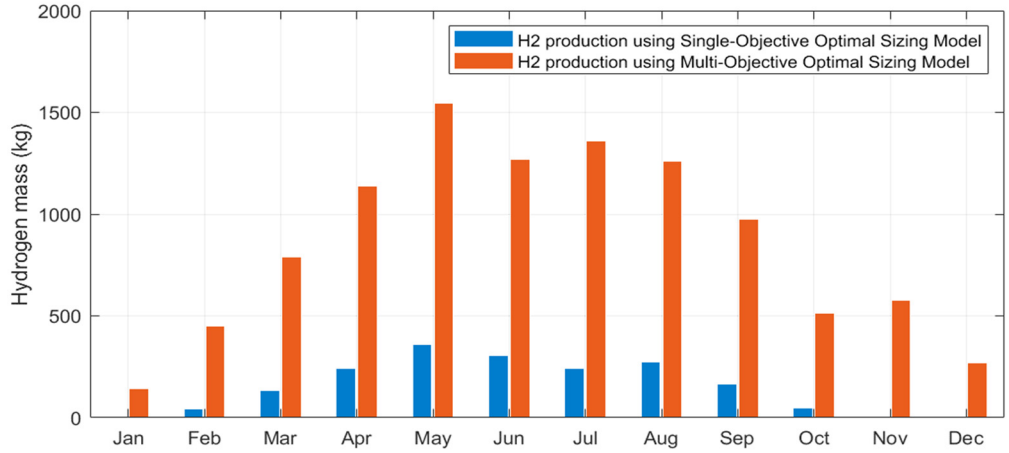


**Figure 7.** Monthly $H_2$ production obtained from the optimal hybrid system sizing when using the single-objective optimal sizing model versus that obtained when using the multi-objective optimal sizing model.

Figure 8 compares the monthly fuel cell energy production obtained from the optimal hybrid system sizing when using the single-objective optimal sizing model versus that obtained when using the multi-objective optimal sizing model. From Figure 8, the annual energy production by the fuel cell system increased from 50.98 MWh when using the single-objective optimisation to 281.73 MWh when using the multi-objective optimisation given that more $H_2$ became available for fuel cell consumption. Indeed, the percentage of annual load demand served by the fuel cell soared from about 3.4% when using the single-objective optimisation to about 18.94% when using the multi-objective optimisation, thus reducing the load dependency on the grid supply and accordingly reducing the environmental impact.

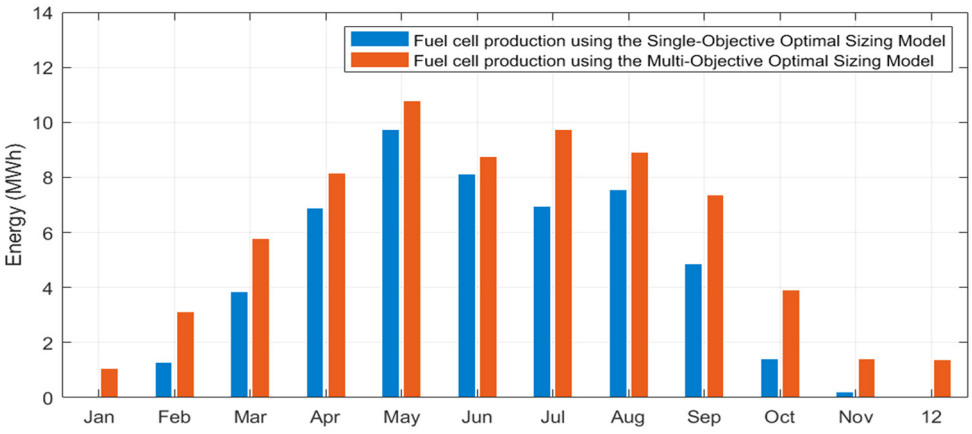


**Figure 8.** Monthly fuel cell energy production obtained from the optimal hybrid system sizing when using the single-objective optimal sizing model versus that obtained when using the multi-objective optimal sizing model.

Figure 9 compares the monthly grid energy import obtained from the optimal hybrid system sizing when using the single-objective optimal sizing model versus that obtained when using the multi-objective optimal sizing model. The annual energy imported from the utility grid decreased from about 900 MWh when using the single-objective optimal sizing model to 495.8 MWh when using the multi-objective optimal sizing model. It is worth stating that the load's grid dependency decreased from about 40% when using the

single-objective optimisation to 33.33% when using the multi-objective optimisation, meaning that about 66.7% of $CO_2$ emissions could be eliminated upon applying the multi-objective optimisation technique.

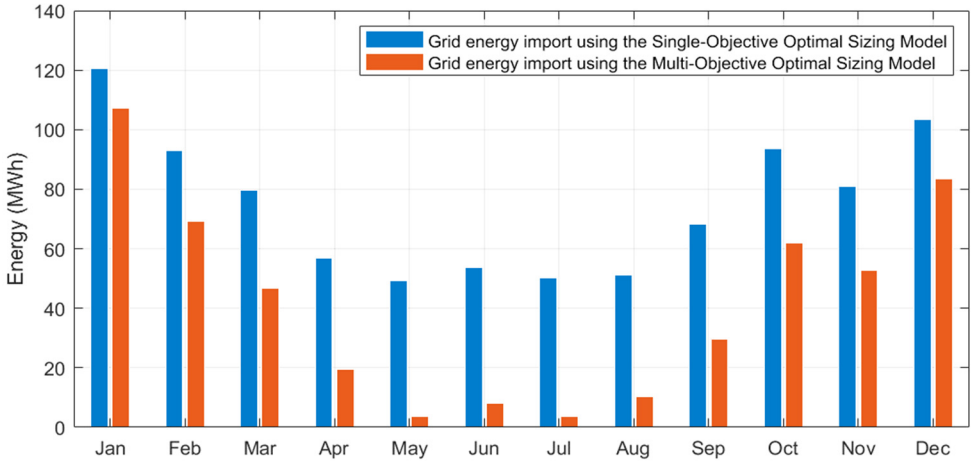


**Figure 9.** Monthly grid energy import obtained from the optimal hybrid system sizing when using the single-objective optimal sizing model versus that obtained when using the multi-objective optimal sizing model.

## 7. Conclusions

In this paper, single-objective and multi-objective optimisation dynamic system models were developed to enable the real-world modelling and the optimal sizing of a hybrid PV-$H_2$ energy system within grid-connected buildings from either an economic perspective only or from economic and environmental perspectives. Both models were developed by implementing the PSO algorithm on the precise dynamic system model that takes into consideration the real-world electrochemical dynamic behaviour of the individual hybrid system components. The results obtained from the single-objective sizing optimisation model attained an economically feasible optimal hybrid system sizing (1000 kW PV system, 932 kW electrolyser, 22.7 kg $H_2$ storage tank, and 242 kW fuel cell system) with a LCOE of 0.366 £/kWh and a grid dependency maintained at 40%. On the other hand, the results obtained from the multi-objective optimisation model realised a more environmentally friendly hybrid system sizing (3187.8 kW PV system, 1000 kW electrolyser, 106.1 kg $H_2$ storage tank, and 250 kW fuel cell system) with a lower grid dependency of 33.33% while holding the LCOE at a slightly higher reasonable value of 0.5188 £/kWh. The analysis of the results obtained from the application of both the single-objective and multi-objective models on the same case study building enabled for envisioning the impact of the optimisation criteria on the conceptual design of the hybrid system.

Further research work should look into optimising the sizing of hybrid renewable-hydrogen energy systems from other perspectives (like maximising the turn around efficiency of the $H_2$ energy conversion to electricity or minimising other sustainability criteria like the water consumption of the electrolyser). It is also recommended to investigate other options for green $H_2$ usage (so instead of converting it back to electricity, it might be more efficient to use it directly for heating purposes or for fuelling vehicles within the building).

**Author Contributions:** Conceptualisation, A.I.A. and D.A.; methodology, A.I.A. and D.A.; software, A.I.A.; validation, A.I.A.; formal analysis, A.I.A.; investigation, A.I.A.; resources, A.I.A. and D.A.; data curation, A.I.A.; writing—original draft preparation, A.I.A.; writing—review and editing, D.A.

and N.S.; visualisation, A.I.A., D.A., and N.S.; supervision, D.A. and N.S.; project administration, D.A.; funding acquisition, A.I.A. and D.A. All authors have read and agreed to the published version of the manuscript.

**Funding:** This research is part of studentship no. ENG20-02 funded by the School of Engineering at Robert Gordon University, Aberdeen, United Kingdom.

**Data Availability Statement:** Data are contained within the article.

**Acknowledgments:** The authors would like to thank RGU Estates for providing the actual load data of the RB to conduct this study.

**Conflicts of Interest:** The authors declare no conflicts of interest.

## References

1. Ceylan, C.; Devrim, Y. Green hydrogen based off-grid and on-grid hybrid energy systems. *Int. J. Hydrogen Energy* **2023**, *48*, 39084–39096. https://doi.org/10.1016/j.ijhydene.2023.02.031.
2. Oyewole, O.L.; Nwulu, N.I.; Okampo, E.J. Optimal design of hydrogen-based storage with a hybrid renewable energy system considering economic and environmental uncertainties. *Energy Convers. Manag.* **2024**, *300*, 117991. https://doi.org/10.1016/j.enconman.2023.117991.
3. Bernoosi, F.; Nazari, M.E. Optimal sizing of hybrid PV/T-fuel cell CHP system using a heuristic optimization algorithm. In Proceedings of the 34th International Power System Conference, PSC 2019, Tehran, Iran, 9–11 December 2019; Institute of Electrical and Electronics Engineers Inc.: Piscataway, NJ, USA, 2019; p. 57–63. https://doi.org/10.1109/PSC49016.2019.9081541.
4. Singh, S.; Chauhan, P.; Singh, N.J. Capacity optimization of grid connected solar/fuel cell energy system using hybrid ABC-PSO algorithm. *Int. J. Hydrogen Energy* **2020**, *45*, 10070–10088. https://doi.org/10.1016/j.ijhydene.2020.02.018.
5. Mokhtara, C.; Negrou, B.; Settou, N.; Bouferrouk, A.; Yao, Y. Design optimization of grid-connected PV-Hydrogen for energy prosumers considering sector-coupling paradigm: Case study of a university building in Algeria. *Int. J. Hydrogen Energy* **2021**, *46*, 37564–37582. https://doi.org/10.1016/j.ijhydene.2020.10.069.
6. Zhang, G.; Shi, Y.; Maleki, A.A.; Rosen, M. Optimal location and size of a grid-independent solar/hydrogen system for rural areas using an efficient heuristic approach. *Renew. Energy* **2020**, *156*, 1203–1214. https://doi.org/10.1016/j.renene.2020.04.010.
7. Gharibi, M.; Askarzadeh, A. Size and power exchange optimization of a grid-connected diesel generator-photovoltaic-fuel cell hybrid energy system considering reliability, cost and renewability. *Int. J. Hydrogen Energy* **2019**, *44*, 25428–25441. https://doi.org/10.1016/j.ijhydene.2019.08.007.
8. Abdelshafy, A.M.; Hassan, H.; Jurasz, J. Optimal design of a grid-connected desalination plant powered by renewable energy resources using a hybrid PSO–GWO approach. *Energy Convers. Manag.* **2018**, *173*, 331–347. https://doi.org/10.1016/j.enconman.2018.07.083.
9. Fonseca, J.D.; Commenge, J.-M.; Camargo, M.; Falk, L.; Gil, I.D. Multi-criteria optimization for the design and operation of distributed energy systems considering sustainability dimensions. *Energy* **2021**, *214*, 118989. https://doi.org/10.1016/j.energy.2020.118989.
10. Fonseca, J.D.; Commenge, J.-M.; Camargo, M.; Falk, L.; Gil, I.D. Sustainability analysis for the design of distributed energy systems: A multi-objective optimization approach. *Appl. Energy* **2021**, *290*, 116746. https://doi.org/10.1016/j.apenergy.2021.116746.
11. Yousri, D.; Farag, H.E.Z.; Zeineldin, H.; El-Saadany, E.F. Integrated model for optimal energy management and demand response of microgrids considering hybrid hydrogen-battery storage systems. *Energy Convers. Manag.* **2023**, *280*, 116809. https://doi.org/10.1016/j.enconman.2023.116809.
12. Modu, B.; Abdullah, M.P.; Alkassem, A.; Hamza, M.F. Optimal rule-based energy management and sizing of a grid-connected renewable energy microgrid with hybrid storage using Levy Flight Algorithm. *Energy Nexus* **2024**, *16*, 100333. https://doi.org/10.1016/j.nexus.2024.100333.
13. Li, C.; Zhang, X. Optimal sizing of hybrid energy storage system under multiple typical conditions of sources and loads. *Int. J. Sustain. Energy* **2024**, *44*, 2439298. https://doi.org/10.1080/14786451.2024.2439298.
14. Lin, L.; Ou, K.; Lin, Q.; Xing, J.; Wang, Y.-X. Two-stage multi-strategy decision-making framework for capacity configuration optimization of grid-connected PV/battery/hydrogen integrated energy system. *J. Energy Storage* **2024**, *97*, 112862. https://doi.org/10.1016/j.est.2024.112862.

15. Nel. *Nel Hydrogen Electrolysers: The World's Most Efficient and Reliable Electrolysers*; Nel: Oslo, Norway, 2019.
16. Pure Energy Centre. PureH2 Hydrogen Electrolyser Available online: https://pureenergycentre.com/hydrogen-products-pure-energy-centre/hydrogen-electrolyser/ (accessed on 23 Jan 2025).
17. Atteya, A.I.; Ali, D. Benchmarking a Novel Particle Swarm Optimization Dynamic Model Versus HOMER in Optimally Sizing Grid-Integrated Hybrid PV–Hydrogen Energy Systems. *Eng* **2024**, *5*, 3239–3258. https://doi.org/10.3390/eng5040170.
18. Atteya, A.I.; Ali, D.; Sellami, N. Precise Dynamic Modelling of Real-World Hybrid Solar-Hydrogen Energy Systems for Grid-Connected Buildings. *Energies* **2023**, *16*, 5449. https://doi.org/10.3390/en16145449.
19. Luna-Rubio, R.; Trejo-Perea, M.; Vargas-Vázquez, D.; Ríos-Moreno, G.J. Optimal sizing of renewable hybrids energy systems: A review of methodologies. *Solar Energy* **2012**, *86*, 1077–1088. https://doi.org/10.1016/j.solener.2011.10.016.
20. Yang, X.-S. Chapter 14—Multi-Objective Optimization. In *Nature-Inspired Optimization Algorithms*; Yang, X.-S., Ed.; Elsevier: Oxford, UK, 2014; pp. 197–211. https://doi.org/10.1016/B978-0-12-416743-8.00014-2.
21. Kennedy, J.; Eberhart, R. Particle swarm optimization. In Proceedings of the ICNN'95—International Conference on Neural Networks, Perth, WA, Australia, 27 November–1 December 1995; Volume 4, pp. 1942–1948. https://doi.org/10.1109/ICNN.1995.488968.
22. Eberhart, Shi, Y. Particle swarm optimization: Developments, applications and resources. In Proceedings of the 2001 Congress on Evolutionary Computation (IEEE Cat. No.01TH8546), Seoul, Republic of Korea, 27–30 May 2001; Volume 1, pp. 81–86. https://doi.org/10.1109/CEC.2001.934374.
23. Bucher, C.; Wandel, J.; Joss, D. Life Expectancy of PV Inverters and Optimisers in Residential PV Systems. In Proceedings of the 8th World Conference on Photovoltaic Energy Conversion, Milano, Italy, 26–30 September 2022; pp. 865–873.
24. EDF. Government Energy Price Guarantee Pricesvailable online: https://www.edfenergy.com/sites/default/files/government_energy_price_guarantee_prices._standard_variable_deemed_and_welcome._credit_meters.pdf (accessed on 24 May 2024).
25. EDF. Smart Export Guarantee. Available online: https://www.edfenergy.com/energy-efficiency/smart-export-tariff (accessed on 24 May 2024).